EPJ Web of Conferences **292**, 12001 (2024) https://doi.org/10.1051/epjconf/202429212001
NRM2023

Medical radionuclide research activities at JRC-Geel

Andrea Tsinganis[1,*], *Pablo* Serra Crespo[2], *Arjan* Plompen[1], *Jan* Heyse[1], *Stephan* Oberstedt[1], *Ana* Ruiz Moreno[3], and *Francesco* Fumagalli[3]

[1]European Commission, Joint Research Centre (JRC), Retieseweg 111, B-2440 Geel, Belgium
[2]European Commission, Joint Research Centre (JRC), Westerduinweg 3, 1755 LE Petten, Netherlands
[3]European Commission, Joint Research Centre (JRC), Via Enrico Fermi 2749, 21027 Ispra (VA), Italy

Abstract. A programme to study photon- and neutron-induced reactions of medical interest, as well as accelerator-based methods of medical radionuclide production, has been instituted at JRC-Geel, making use of both existing and new infrastructure. A new electron beamline that can deliver quasi-mono-energetic beams has been commissioned at the GELINA electron linac and will be primarily dedicated to the study of photonuclear reactions and for medical radioisotope production studies via photon irradiation. The recently renewed MONNET 3.5 MV Tandem accelerator provides light ion beams for reaction-based quasi-mono-energetic neutron production and has been used for the study of ^{99}Mo production via neutron irradiation of molybdenum nanoparticles. In this work we present an overview of the medical radionuclide activities at JRC-Geel, with particular attention to aspects of the design, development and operational challenges of the new GELINA electron beamline. Some future perspectives of the programme are also discussed.

1 Introduction

Radioactive nuclides are routinely used for medical procedures, including both imaging and treatment. At least part of the demand for medical radionuclides currently produced via fission of ^{235}U in dedicated reactors could be met in the future by alternative accelerator-based production routes via photonuclear, neutron, and light-ion reactions, thus addressing supply chain issues that arise from the operation of ageing reactors and nuclear proliferation concerns, as well as offering easier separation of the end-products and a reduced reliance on a limited number of large producers.

In this context, a programme to study photon-induced reactions of medical interest, as well as accelerator-based methods of medical radionuclide production, has been instituted at JRC-Geel (Belgium). Making use of existing as well as new infrastructure, this activity focuses on both established radionuclides, such as ^{99m}Tc and its parent ^{99}Mo (used in SPECT imaging), and emerging radionuclides, such as ^{225}Ac (relevant for targeted alpha therapy).

2 The new electron beamline for photonuclear reaction studies

The GELINA facility [1] at JRC-Geel has for decades been dedicated to the production of pulsed neutron beams spanning several orders of magnitude in energy for nuclear data

*e-mail: Andrea.TSINGANIS@ec.europa.eu

measurements (via time-of-flight technique) relevant for nuclear energy applications and nuclear decommissioning. Neutrons are produced by an electron beam accelerated by a linac impinging on a mercury-cooled rotating depleted uranium target. The impact leads to Bremsstrahlung production which induces photonuclear reactions in the uranium, thus generating neutrons. The (fast or moderated) neutrons enter various flight-paths (in vacuum) and reach experimental cabins located at different distances, from a few metres up to 400 m, where a variety of experimental setups study their interactions with materials.

A new electron beamline that can deliver quasi-mono-energetic beams between 20-130 MeV has been commissioned at GELINA and will be primarily dedicated to the study of photonuclear reactions and for medical radionuclide production studies via photon irradiation. The photon beams are produced via Bremsstrahlung from the electron beam impact on a high-Z radiator consisting of Pb disks of 2 mm thickness each. The number of disks can be adapted to the needs of a particular irradiation. The new beamline is located in the GELINA target hall, which houses the pre-existing straight beamline leading electrons through the compression magnet [2] and finally to the uranium target for neutron production. The main components of the new beamline are two bending magnets used to deflect the beam off the straight line and towards a dedicated irradiation station. The location of the new beamline inside the target hall is shown in Fig. 1.

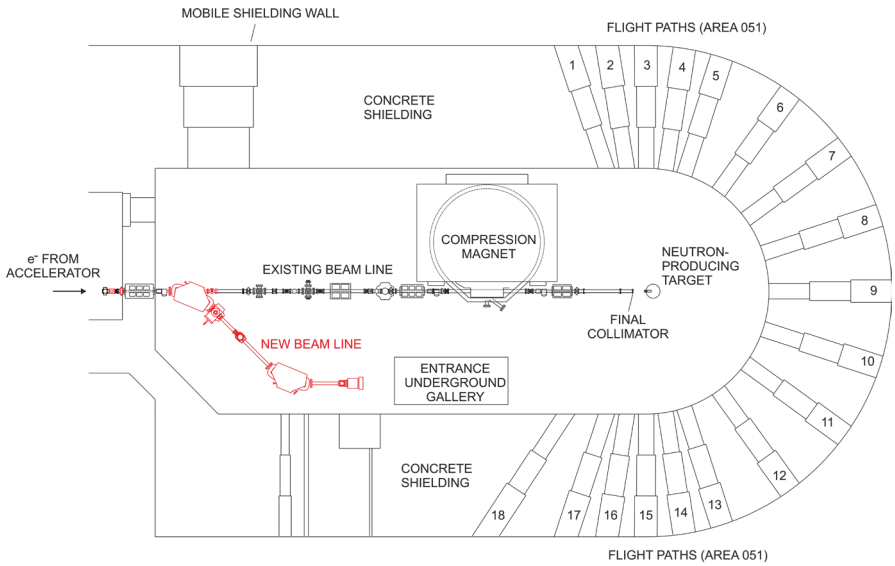

Figure 1. Diagram of the GELINA target hall. In red, the components of the new beamline.

2.1 Beamline layout

The first bending dipole is integrated in the pre-existing straight beamline and is installed immediately after the point where the beamline transporting the accelerated electron beam enters the target hall. It deflects the incoming electron beam to the right with respect to the existing beamline, while the second dipole deflects the electron beam in the opposite direction and transports the electron beam to an irradiation setup. The combination of the two dipoles provides the required electron energy selection. A more detailed view of the new beamline and its individual components is shown in Fig. 2.

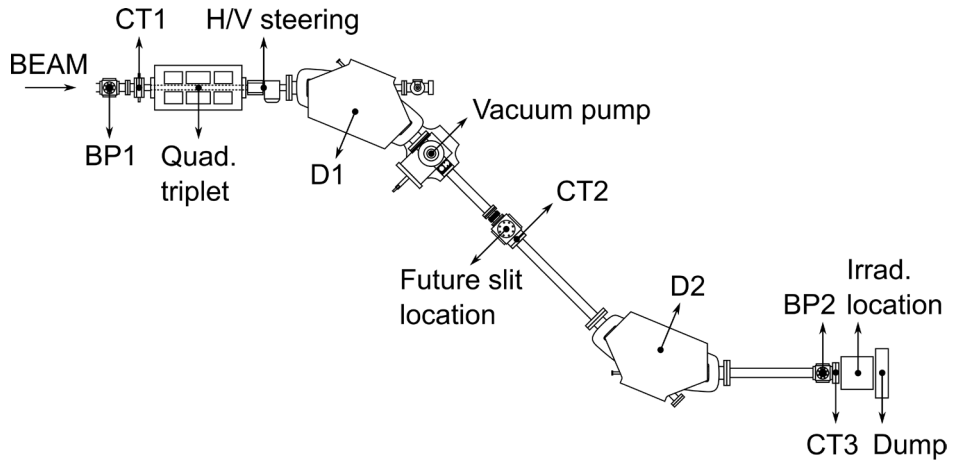

Figure 2. Diagram of beamline components (beam entering from the left). BP: beam profile monitors. CT: current transformers (FCT/ICT pairs). D1, D2: bending dipoles. Details in the text.

The 0.5 T bending dipoles (D1, D2 in Fig. 2) have a bending radius R of 1.15 m and a bending angle θ of 45°. They have an almost identical behaviour with a slope of approximately 5.6 mT/A. Hysteresis was also found to be very low, with a residual field of approximately 2 mT after a cycle from 0 to 100 A and back. The electron beam at the exit of the second dipole is parallel to the initial direction before entering the beamline and at a distance of 2.3 m (i.e. twice the bending radius R) from the straight beamline.

Preceding the first bending dipole are a quadrupole triplet and a pair of steering magnets. All these magnets were pre-existing on the line at a slightly different location and can be used to optimise the beam entering the beamline. The quadrupoles can control the beam focusing at the irradiation location, while the steering magnets are useful in correcting any small misalignment of the beam with respect to the centre of the beam profile monitor at the end of the beamline (BP2).

2.2 Beam optics

First-order beam optics calculations were performed in order to study the evolution of the transverse beam profile along the beamline. This is important for identifying potential beam loss locations and determining operational constraints. From such an analysis it emerges that, assuming realistic values for the beam size (of the order of 1 cm diameter) and divergence (below 1 mrad) at the entrance of the beamline, the momentum spread is by far the dominant factor in increasing the transverse beam size (on the horizontal plane). The first dipole acts as an energy analyser and beam losses can begin to occur well before the beam enters the second dipole, which recombines the beam at the focal point. The calculated beam envelope in the horizontal and vertical plane for a specific configuration is shown in Fig. 3. The beam size at this location is very close to the initial one (although the divergence is significantly higher). For this reason, this is chosen as the location for the radiator and samples.

Monte Carlo simulations carried out with FLUKA [3, 4], implementing the above beam optics and tracking the electron beam in a realistic geometry of the beamline (Fig. 4, left), showed that the momentum acceptance of the beamline is approximately ±1.5%. An example of a loss map generated for a specific optics configuration is also shown in Fig. 4 (right).

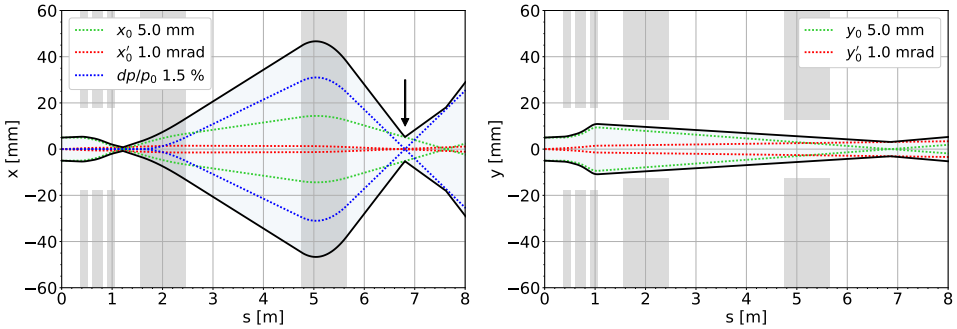

Figure 3. Calculated beam envelope on the horizontal (left) and vertical (right) planes for a specific optics configuration. The assumed initial beam parameters (radial dimension, divergence and momentum spread) are given in the legend. Shaded areas represent the quadrupole triplet and the two bending dipoles. The bending dipoles only act on the horizontal plane. Contributions by individual beam parameters are also shown, highlighting the dominant contribution of the beam momentum spread (blue curve). The position of the focal point is marked with an arrow.

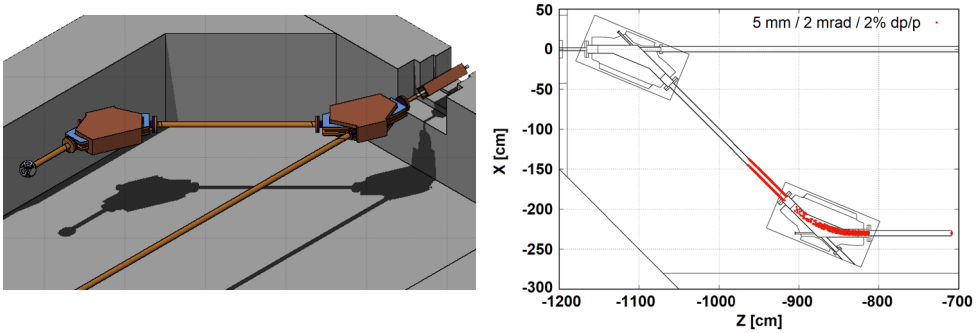

Figure 4. Left: A 3D view [5] of the FLUKA model of the beamline inside the GELINA target hall. Right: beam loss map generated for a given optics configuration and specific beam parameter assumptions.

2.3 Electron beam profile and beam current

Two beam profile monitors, one in front of the first dipole (BP1) and one just before the irradiation station (BP2) are used to visualise the electron beam-spot. These monitors consist of thin aluminium foils (250 μm), with the normal to the foils rotated by 45° with respect to the beam. When the electrons impinge on these aluminium discs, optical transition radiation [6] is produced at the boundary between the vacuum and the foil and is captured by a camera.

The beam profile monitor at the end of Section 3 of the linac (i.e. at the entrance of the beamline, BP1) can be remotely inserted into position to check the beam-spot and is observed via a camera placed directly above it, inside the accelerator gallery. The beam profile monitor before the irradiation station (BP2) is permanently in place and is observed with a camera located in the annex adjacent to the target hall via two mirrors and a water-filled wall penetration since the radiation levels inside the target hall during operation are too high for the camera's electronic components. Markings of known dimensions are present on

the foils and are used to calibrate the camera images by using images captured without beam and with the lights on. The image calibration is given in units of μm per pixel and is typically around 40-45 μm/px, offering more than sufficient resolution for reconstructing the beam-spot profile from the recorded images. The viewing parameters of the cameras (alignment, focus, field of view) are optimised prior to accelerator start-up and remain unchanged throughout the measurement campaign. Examples obtained at the beamline exit (BP2) are shown in Fig. 5.

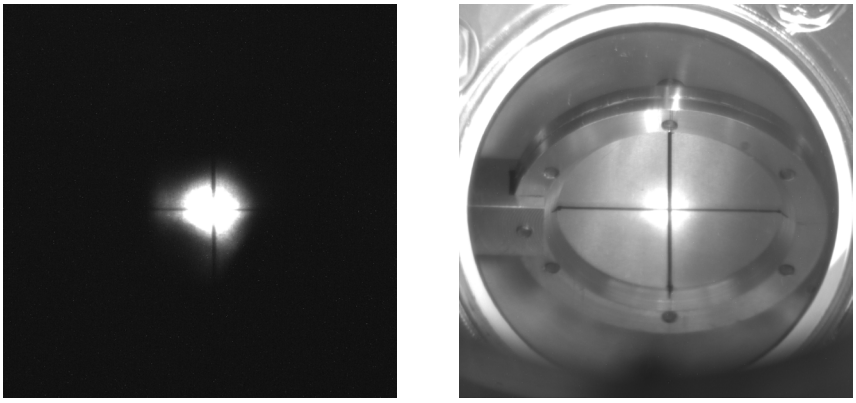

Figure 5. Left: An image of the electron beam obtained on the beam profile monitor screen located just before the exit of the beamline (BP2 in Fig. 2), for an electron energy of about 130 MeV, with 16 nC/bunch at 10 Hz repetition rate, and 1 s camera exposure time. Right: the beam profile monitor as seen with the target hall lights on. With the above beam parameters, the spot is bright enough to still be visible with the lights on, which is not the case for electron energies below several tens of MeV. The cross is 5 cm wide and the beam is contained within about 15 mm.

The electron beam intensity is measured using current transformers. To determine the fraction of the beam transported through the line (and consequently any beam losses occurring), current transformers are installed before the first dipole (CT1), between the two dipoles (CT2) and just before the irradiation station (CT3). At each location there is an FCT (Fast Current Transformer), which gives a fast signal whenever a beam bunch passes allowing to observe the time-structure of the bunch, and an ICT (Integrating Current Transformer), a calibrated device that outputs a long signal proportional to the total charge of each beam bunch. The ICT value recorded at the end of the beamline (CT3) is the one used to determine the beam integral delivered on target during an irradiation.

2.4 Electron beam energy

The linac consists of three accelerating sections. Section 1 is a 2.25 m long standing wave cavity which sets the beam bunch structure and accelerates electrons up to an energy of about 20 MeV, while Sections 2 and 3 are 6 m long travelling wave cavities, each adding about 55 MeV of energy to the electrons for a total of 130 MeV at the exit of Section 3. Once the desired electron energy is chosen, the currents of the bending dipoles are accordingly set. At that point, the high voltage applied to Sections 2 and 3 (the latter only if required) are adjusted in order to reduce or increase the beam energy, as needed. The beam current at the entrance (CT1), midpoint (CT2) and exit (CT3) of the beamline are monitored until a maximum current value is reached, which generally requires adapting the optics along the entire accelerator, as well as the phase differences between sections.

In neutron production mode, the linac is operated with a high current (100 μA average) and very short pulses (10 ns), essential for time-of-flight experiments. In these conditions, the depletion of the RF power in the sections leads to a very large energy difference between leading and trailing electrons in a bunch that emerge with energies of about 130 and 70 MeV respectively, corresponding to an energy spread of ±30%. It is therefore evident from the optics considerations above (Sec. 2.2), that operating the new beamline poses far more stringent conditions on the parameters of the accelerator. In particular, a lower and slower depletion of the RF power in the linac sections and therefore a lower beam energy spread can be achieved by a reduction of the injected charge per bunch and a lengthening of the beam pulse. Based on recent experience, no more than 100 nC/bunch are injected and the pulse length has been increased to about 2.0-2.5 μs. The average current at the beamline exit ranges from a few hundred nA to 1-2 μA, still sufficient for activation of foils within a few minutes.

While reduction of the energy spread to about ±1.5% (i.e. about ±1 MeV at 70 MeV electron energy) and complete elimination of beam losses in the beamline may not be ultimately achievable, it is nevertheless important to reduce the energy spread to no more than a few percentage points, limiting losses to the part of the beamline between the two dipoles and at the entrance of the second one, where a future slit system or permanent collimator could allow to intercept off-momentum electrons in a controlled way.

In order to investigate the electron beam energy spectrum, the current applied to the first dipole (D1) was automatically ramped up at a slow rate of 0.1 A/s, while the values of the ICT at the beamline midpoint (CT2) were simultaneously recorded. Although some beam losses were observed between the ICTs at the NBL entrance (CT1) and the midpoint (CT2), this spectrum is the closest observation that can be made of the energy distribution of the beam delivered by the linac. The example shown in Fig. 6 was obtained with a central electron energy of 61 MeV, a pulse length of 2 μs and an injected beam charge of 31 nC. Subtracting the baseline, we observe a peak charge of about 22 nC, indicating that beam losses occur even before the midpoint, with about 70% of the initial beam surviving. The energy distribution displays a width σ of about 2.1 MeV, corresponding to a spread of ±3.4% in beam energy.

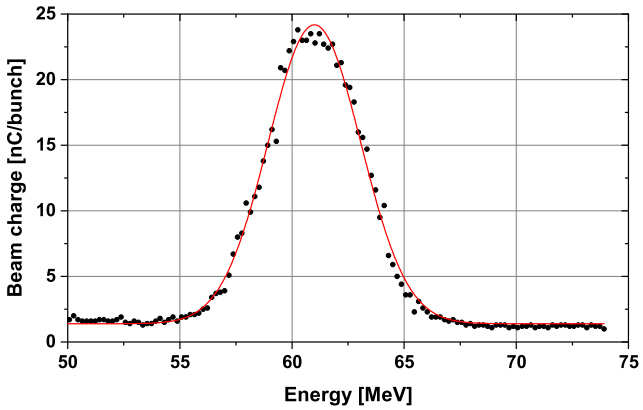

Figure 6. Electron beam energy spectrum obtained at the midpoint between the two bending dipoles, with a central electron beam energy of 61 MeV, a pulse length of 2 μs and an injected beam charge of 31 nC/bunch, using the method described in the text. A Gaussian fit of the distribution is also shown.

3 Production of radionuclides via nanoparticle irradiation

The main objective of the *ir-NANO* project is to develop a new production route for high specific activity ^{99}Mo via the ^{100}Mo(γ,n), ^{100}Mo(n,2n) or ^{98}Mo(n,γ) reaction using molybdenum in nanoparticle form. The basic idea is that primary recoils can escape from the nanoparticles if their size is smaller than the range of the recoils, and then be chemically extracted.

The nanoparticles are produced at JRC-Petten (Netherlands) by spark ablation of natural molybdenum electrodes (9.74% ^{100}Mo) followed by gas-phase nucleation and growth in an inert gas flow which determines the size of the nanoparticle agglomerates. As shown in Fig. 7, agglomerates of over 200 nm are formed with an argon flow of 1 L/min, while at 2 L/min the agglomerates are about half this size. At 5 L/min, still smaller agglomerates are mixed with small particles. With a flow of 10 L/min no agglomerates are visible and only nanoparticles are produced. In contrast to discrete nanoparticles, agglomerates can be easily separated by centrifugation, therefore a flow of 2 L/min was chosen for further sample preparation.

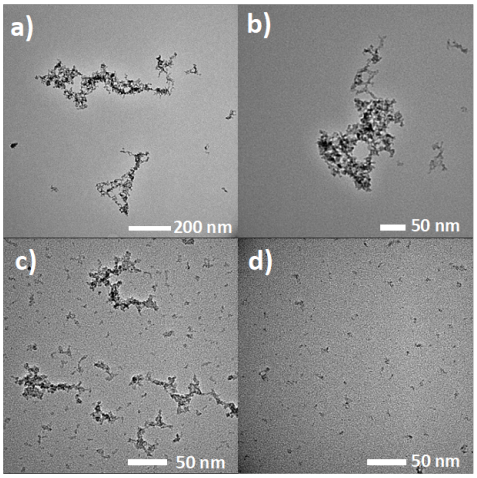

Figure 7. Molybdenum oxide nanoparticles produced by spark ablation with an argon flow of a) 1 L/min, b) 2 L/min, c) 5 L/min and d) 10 L/min. A flow of 2 L/min was finally chosen, as discussed in the text.

Fast neutron irradiations of molybdenum oxide nanoparticle samples have been carried out at the MONNET 3.5 MV tandem van de Graaff light ion accelerator in JRC-Geel. MONNET [7] provides continuous or pulsed light ion beams (protons, deuterons) that can be used to produce quasi-mononergetic neutrons via different nuclear reactions, with fluxes between 10^6 n/(s·sr) and 10^9 n/(s·sr). For these irradiations, neutrons of around 15.5 MeV (matching the maximum of the ^{100}Mo(n,2n) reaction cross-section) were produced via the ^{3}H(d,n) reaction by a deuteron beam of around 820 keV impinging on a tritiated titanium target. The sample mass was 20.6 mg/sample on average (corresponding to 1.35 mg of ^{100}Mo). The samples were placed near the neutron source in order to maximise the flux. Irradiations of two samples at a time lasted up to 24 h and the neutron flux was monitored with ^{3}He counters. The average integrated flux delivered on each sample was 5.7×10^{11} cm^{-2} and the average induced ^{99}Mo activity per sample was 18 Bq.

After irradiation, the samples were dispersed in different extraction solutions, which included typical metallurgy extracting agents. The choice of solvent used for the solid-liquid extraction has to prevent dissolution of the nanoparticle agglomerates that would result in a reduction of the final specific activity. Molybdenum oxide agglomerates are not stable in water; chloroform was therefore preferred as solvent, while octanol was tried and discarded.

The induced ^{99}Mo activity was determined using High-Purity Germanium (HPGe) detectors. In the subsequent step, the bulk nanoparticles are separated by centrifugation and the eluate is again measured to determine the extracted ^{99}Mo activity. It is further subjected to elemental analysis characterisation techniques at JRC-Ispra (Italy) to determine the extraction yield and the specific activity. Under some of the extraction conditions, a selective isotopic separation of ^{99}Mo was accomplished, resulting in an increased specific activity by factors of a few hundred in the best cases. First results will be published in the coming months.

4 Summary and Perspectives

Successful beam transmission through the new electron beamline at GELINA has been achieved at different electron energies spanning the range from below 20 to over 130 MeV, while remaining well within the defined safety envelope of the facility. A first series of irradiations of ^{nat}Mo foils has been performed at energies spanning the entire range of the linac. The results are being analysed and will also be used to validate the Monte Carlo model of the beamline and irradiation station. Further improvements to beam instrumentation (such as a Faraday cup for accurate currrent measurement and a slit system or collimator for the interception of off-momentum electrons) are being developed and will offer improved control of beam parameters in the future.

Selective extraction of ^{99}Mo from neutron-irradiated molybdenum nanoparticles has been demonstrated in the context of the ir-NANO project. Further optimisation of the nanoparticle production, and irradiation and extraction procedure is required in order to maximise the enrichment factors and scale-up the process. The alternative route via ^{100}Mo(γ,n) can be investigated at the new GELINA beamline in the future. With the same underlying principle, a first neutron-irradiation of radiation-resistant chromium metal-organic frameworks (MOFs) [8] has been recently performed at MONNET to investigate the possibility of developing a similar procedure for production of ^{51}Cr, a radionuclide used as a red blood cell label and currently produced via neutron activation in reactors.

Finally, a collaboration with SCK-CEN (Belgium) is ongoing for production of ^{225}Ac via photon irradiation of ^{226}Ra. Dummy samples were irradiated at the GELINA beamline in anticipation of the actual experiments, and a complementary campaign is planned at γ-ELBE (Germany) [9] to cover the low energy range below 20 MeV, which is of particular interest.

Acknowledgements

The authors wish to acknowledge the fundamental contribution of the entire GELINA and MONNET operator teams, especially those involved in developing instrumentation and operational parameters and procedures for the new GELINA beamline.

References

[1] A. Oprea et al., EPJ Web Conf. **284**, 06005 (2023)
[2] D. Tronc, J. Salomé, K. Böckhoff, Nucl. Instrum. Meth. A **228**, 217 (1985)
[3] C. Ahdida et al., Front. Phys. **9** (2022)
[4] G. Battistoni et al., Ann. Nucl. Energy **82**, 10 (2015)
[5] V. Vlachoudis, *FLAIR: A powerful but user friendly graphical interface for FLUKA*, in *Proc. of Intl. Conf. on Mathematics, Computational Methods and Reactor Physics* (American Nuclear Society, Saratoga Springs, New York, 2009), pp. 790–800
[6] P. Goldsmith, J.V. Jelley, Philos. Mag. A **4**, 836 (1959)
[7] C.L. Fontana, C. Bonaldi, W. Geerts, M. Macías Martinez, M. Vidali, S. Oberstedt, EPJ Web Conf. **284**, 06002 (2023)
[8] S. Dutt, A. Kumar, S. Singh, Clean Technologies **5**, 140 (2023)
[9] R. Schwengner, R. Beyer, F. Dönau, E. Grosse, A. Hartmann, A. Junghans, S. Mallion, G. Rusev, K. Schilling, W. Schulze et al., Nucl. Instrum. Meth. A **555**, 211 (2005)